Batteries & Supercaps

Research Article
doi.org/10.1002/batt.202200524

Chemistry Europe
European Chemical Societies Publishing

www.batteries-supercaps.org

Quantitative Cell Classification Based on Calibrated Impedance Spectroscopy and Metrological Uncertainty

Amin Moradpour,[a] Manuel Kasper,[a] and Ferry Kienberger*[a]

Electrochemical impedance spectroscopy (EIS) is widely used for battery cell testing in industrial production and R&D labs. This work addresses the use of EIS calibration and uncertainty analysis in cell classification. Five scenarios are investigated to discuss qualitatively the impact of calibration and uncertainty on classification. For an experimental demonstration, a cylindrical cell was measured with two mechanical fixtures of different qualities and characterized regarding random errors and calibrated impedances. The impact of uncertainty and impedance calibration on the cell classification is shown, and based on the uncertainty and corresponding error bounds, a confidence level was established for the classification results. Quantitative uncertainty bounds are presented for the full EIS frequency spectrum ranging from 150 mHz to 5 kHz.

Introduction

Batteries are a critical element in the global transition to green energy. The battery production industry is rapidly growing, with expansion plans in place to reach a total production of 6 TWh by 2030,[1] which translates to billions of standard cylindrical cells, assuming typical 3.5 Ah with a nominal voltage of 3.7 V. Batteries are expected to fulfill a range of quality criteria depending on the application type, such as high power density, long cycle life, and low self-discharge. However, it is also essential that these criteria are achieved with high consistency. A single underperforming cell can drag down the performance of a full electric vehicle (EV) battery pack, and a single defective cell may pose a safety risk. Therefore, testing of cells before they leave the factory is critical for cell manufacturing Gigafactories, and similarly, cells are tested also at automotive manufacturers before they are integrated into modules and packs. Various tests are conducted during the entire production chain in order to evaluate the different parts of a cell as well as the completely formed cell. For example, a voltage breakdown test can be performed to determine the quality of the polymeric separator layer in an R&D pilot line,[2] and electrochemical impedance spectroscopy (EIS) is typically used to determine the overall electrochemical performance and impedance characteristic of the completely assembled cell.[3] Several prognostic studies employing EIS to characterize battery performance at different operational conditions have been reported. For example, EIS was applied for cell quality assessment,[4] state of charge (SoC)[5] and state of health (SoH) estimation,[6] temperature monitoring,[7] power fading characterization,[8] and electrochemical aging of batteries.[9]

Impedance values can be used as an SoH test of a battery cell,[10] particularly when the impedance is independent of SoC.[11] For instance, in Ref. [11b], the SoH is evaluated at the frequency point where the EIS curve crosses the real axis of the Nyquist plot, which is typically between 500 Hz and 1.5 kHz,[12] and where the ohmic resistance value is mostly independent of SoC. In Ref. [13], EIS data is used to predict the equivalent circuit model and provide input to a neural network in order to simplify the complexity of manual feature extraction. In Ref. [14], EIS at different frequencies was used to evaluate the SoH using different methods including linear regression and distribution of relaxation time analysis.

Recently, the demands in automotive applications for rapid battery charging and high battery performance led to continuous improvement in cell chemistry and cell construction. Consequently, the internal impedance of a single cell has dropped to very low values, and today the cell impedance variations that are of interest for EIS can be as low as a few micro-Ohms (μΩ). The frequency range of interest in EIS is typically very wide, ranging from 1 mHz up to 10 kHz and beyond. In EIS, the DUT is excited by a sinusoidal current with a specific frequency, and the voltage response is recorded. The complex impedance is then calculated using the recorded voltage and current at that particular frequency. In EIS, the measurements are typically affected by two error sources, including random errors and systematic errors. Systematic errors are stationary and typically caused by imperfect instrument calibration and environmental interference and should be removed from the measured data with a proper calibration technique.[3,15] Random errors arise from unpredictable changes during an experiment, such as instrument electronic drift, electromagnetic interference, random position of the fixture, or physical fixture and cable movements. Since random errors have random characteristics, they can not be removed from the result with calibration. However, their effect can be shown by defining the uncertainty bounds of the calibrated measurements.[16]

[a] A. Moradpour, M. Kasper, Priv. Doz. Dr. F. Kienberger
Keysight Laboratories,
Keysight Technologies Austria GmbH
Linz 4020 (Austria)
E-mail: Ferry_kienberger@keysight.com

The consequence of testing methods having an error and an uncertainty is that there are false negatives, an unacceptable cell erroneously passing inspection, and false positives, an acceptable cell erroneously rejected. Therefore, an acceptance threshold must be chosen that balances between both errors. Avoiding false negatives is generally more critical, but the financial and environmental cost of reducing production yield through false positives in testing is not negligible either. Reducing the prevalence of false positives in classification by a small percentage has substantial real-world impact on the efficiency of Gigafactories.[17]

In all EIS studies presented so far, the impedance uncertainties were not fully characterized. Recent studies[3,16] show that systematic and random errors increase significantly with frequency, leading to considerable errors in impedance measurements. Unlike systematic errors, random errors and corresponding uncertainty can not be removed by calibration and need to be experimentally characterized. Uncertainty is highly affected at lower frequencies because of the flicker noise which is proportional to 1/*f*, and at higher frequencies, the impact of repeatability and other noise sources are dominant in the uncertainty. In this work, we therefore aim to improve cell classification that is based on EIS by two means. First, by employing EIS calibration to remove the systematic errors from the measured impedance. Second, by providing measurement uncertainty and confidence levels of the calibrated impedance. The calibration and uncertainty characterization methodology is described, and the quality of the fixture and the effect on the cell classification is explained. Examples of five different hypothetical scenarios in using EIS measurements for cell classification are provided. Original EIS measurements are shown, including raw data, calibrated data, and uncertainty bounds for two different fixtures, as well as the impact on the cell classification.

Methods

EIS calibration and uncertainty propagation

Figure 1 shows sources of uncertainty in EIS measurements and the propagation of uncertainty in different stages of measurement and analysis. A brief account is given in the following, with a detailed mathematical description available in the previous study.[16] First, various uncertainty sources are identified and characterized using multiple measurements on a short standard and a shunt standard. We characterized the effect of measurement repeatability uncertainty and measurement noise uncertainty as being the two primary random error sources. Second, the characterized uncertainties are combined with the DUT raw EIS measurements and the calibration standards measurements and uncertainties are propagated using a linear propagation method through the different calibration and correction functions. This results in the final calibrated impedance and corresponding uncertainties. Since the impedance is composed of a real and an imaginary part, the uncertainty is provided as a 2×2 covariance matrix for each frequency point, where the diagonal elements determine the variances for the real and imaginary components of the calibrated impedance. This covariance matrix is later used in cell classification and error visualization within the Nyquist plot.

The calibration process uses a three-term technique to remove systematic errors from the measured EIS raw quantities.[3,15b] Calibration is performed over the frequency range of 150 mHz to 5 kHz and uses three standards, including one short standard with zero impedance in all frequencies and two resistors of known resistance values (10 mΩ and 50 mΩ). The nominal resistance values of shunt standards have been measured by a calibrated Keysight 3458A Digital Multi Meter (DMM) with an accuracy of ±50 μΩ over a one-year calibration interval. That translates into an accuracy of 0.5% and 0.1% for the 10 mΩ and 50 mΩ shunts, respectively. The systematic error of the measured impedance (Z_m) contains three contributions, a series impedance (Z_{ser}), a parallel conductance (Y_{par}), and the gain (G). The true impedance of the DUT (Z) is given as:[3]

$$Z = \frac{Z_m}{\left(G - Y_{par}.Z_m\right)} - Z_{ser} \tag{1}$$

Three standards of known values (short, 10 mΩ, and 50 mΩ) are used for obtaining the three unknown error coefficients (Z_{ser}, Y_{par}, and G). To calculate the error coefficients, we define three intermediate variables as follows:

$$k_1 = Z_{ser} + \frac{1}{Y_{par}}\ ,\ k_2 = \frac{G}{Y_{par}}\ ,\ k_3 = \frac{Z_{ser}G}{Y_{par}} \tag{2}$$

The following matrix equation is solved to find k_i:

$$\begin{bmatrix} Z_{m1} & -Z_{d1} & -1 \\ Z_{m2} & -Z_{d2} & -1 \\ Z_{m3} & -Z_{d3} & -1 \end{bmatrix} \begin{bmatrix} k_1 \\ k_2 \\ k_3 \end{bmatrix} = \begin{bmatrix} -Z_{m1}.Z_{d1} \\ -Z_{m2}.Z_{d2} \\ -Z_{m3}.Z_{d3} \end{bmatrix} \tag{3}$$

Each row consists of the measured value Z_{mi} and the definition value Z_{di} of the calibration standard '*i*'. The true impedance results are calculated by correcting the measured impedance using the three error coefficients as stated in Equation (1). The calibration

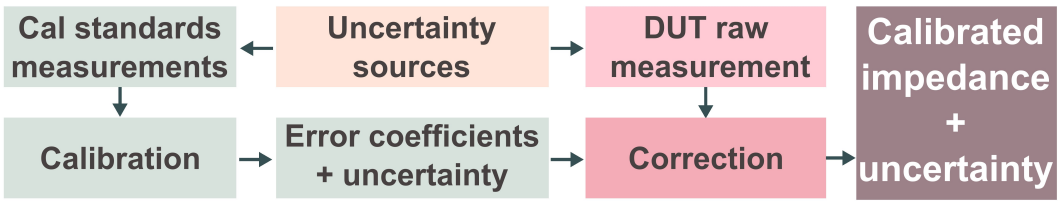

Figure 1. Uncertainty propagation in battery EIS. The uncertainties for calibration standards and DUT measurements are measured and propagated to the final impedance. Error coefficients are calculated, and the raw impedance measurements are corrected. This results in calibrated impedances, including real and imaginary parts, and their uncertainty in the form of a 2×2 covariance matrix.

Research Article
doi.org/10.1002/batt.202200524
Chemistry Europe
European Chemical Societies Publishing

effect becomes more dominant at higher frequencies where the systematic errors increase significantly for instance due to cables or nonlinearity effects in the hardware. A previous study[3] reported that significant systematic-error corrections are obtained from the calibration. For instance, a correction of the raw data of one order of magnitude is applied for the reactance (i.e., inductance) and more than 100% for the resistance at 1 kHz.

Effect of fixture quality on the uncertainty of repeatability

One significant uncertainty source in EIS is mechanical fixture repeatability. Several measurements were performed on two different fixtures (good and bad) to characterize the fixture repeatability uncertainty, including recontacting, mechanical connector reconnection, and arbitrary cable movements. Here, 40 cycles of recontacting and reconnection were done for each fixture. If the fixture is not optimally designed (see Figure 2, bad fixture), it introduces random errors in each recontacting and reconnection cycle, resulting in significant uncertainty in the impedance results. The good fixture has an optimized mechanical holding mechanism to keep the cell in the same position with respect to the fixture contacts, therefore, introducing more repeatable measurements with less uncertainty.

Measurement setup and DUT

For the cylindrical cells, a module tester (Keysight SL1001 A) is used to supply the sinusoidal current and voltage, and the Keysight Energy Storage Discover (ESD) software is used to control the hardware and record the EIS results. The tester is connected to the DUT by a Kelvin connection that is used to separate force and sense wires. The sense and force terminals from the hardware are connected to the fixture via coaxial cables. The experiments are performed on two different fixtures for a cylindrical cell in the frequency range of 150 mHz to 5 kHz on a total of 20 points. The classification is evaluated based on the impedance value at a single frequency point of 1500 Hz. The EIS measurements for the prismatic cells were done with a source measurement unit (SMU) installed on a power analyzer mainframe to supply the sinusoidal current and record the voltage response and the applied current. The signal generation block consists of a sinusoidal current source and a power amplifier to deliver the current to excite the DUT. An additional SMU is used for voltage compensation of the battery cell.

Results and Discussion

Calibration and uncertainty for cell classification

In EIS, two error sources dominate, including systematic and random errors. For systematic errors, output results are typically not fully calibrated in conventional EIS studies, and the effects of metrological calibration and systematic errors are often overlooked. Random errors and corresponding uncertainty analysis haven't been considered in EIS so far and have been introduced only recently.[16] Here we integrate full EIS calibration and metrological uncertainty analysis to show how error correction and uncertainty affect battery cell classification (see Figure 3). Also, the effect of using two fixtures on uncertainty evaluation and cell classification of different qualities is shown. Figure 3 shows a sketch of five different cell EIS raw measurements (blue arrows) and how calibration and uncertainty influence their classification into good (left), intermediate (middle), and bad (right) cells. The effect of the two fixtures is shown on the error bounds of the calibrated measurements. Systematic errors are corrected by the calibration process (black arrows). Random errors determine the measurement uncertainty, which are shown as ellipsoids around each calibrated impedance point. In this sketch, fixture #1 has a better quality than fixture #2, resulting in smaller ellipsoids for fixture #1 (yellow ellipses) and larger ellipsoids for fixture #2 (black dashed ellipses).

For the five different cases we analyze the effects of calibration and uncertainty on the classification as good, intermediate, and bad cells (see also Table 1). In case 1, the raw impedance is classified as good, while by removing the

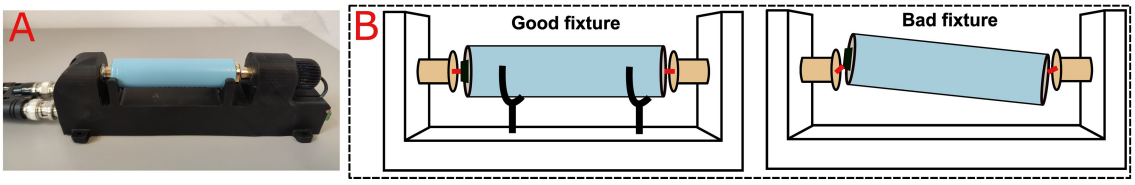

Figure 2. Cylindrical cell fixtures. A) Picture of the optimized battery fixture holding a cylindrical cell. B) Sketch of a good fixture (left) where the positioning and mechanics ensure that the cell keeps its orientation and position during multiple placing and removing cycles. In a bad fixture (right) the positioning is less repeatable, adding uncertainty to the measurements.

Table 1. Cell classification for the five cases, including calibration and uncertainty values. The initial classification is modified based on calibration and uncertainty knowledge. The CL is given in each case.

Case	Initial classification using raw data	Final classification using calibration & uncertainty	Calibration affects classification	Uncertainty affects classification
1	Good	Intermediate	Yes	Yes
2	Good	Intermediate	Yes	No
3	Intermediate	Intermediate	No	No
4	Intermediate	Bad	Yes	Yes
5	Intermediate	Intermediate	No	Yes

Research Article
doi.org/10.1002/batt.202200524
Chemistry Europe
European Chemical Societies Publishing

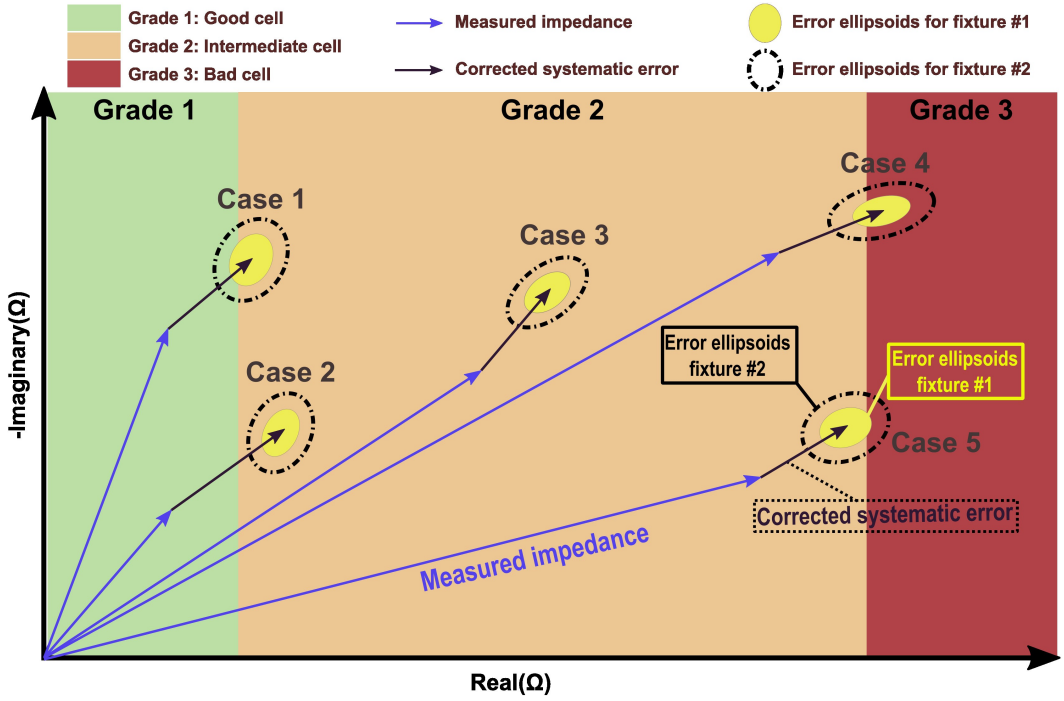

Figure 3. Accurate cell classification based on EIS calibration and uncertainty analysis. Examples of five hypothetical cells include EIS raw data (blue arrows), calibrated EIS data (black arrows), and uncertainty boundaries for two different fixtures (good fixture in yellow ellipsoids and bad fixture in black dashed ellipsoids). In all cases except case #3, the classification of good (left), intermediate (middle), and bad (right) cells is affected at least by the calibration or by the uncertainty.

systematic error via calibration, the resulting impedance moves to class intermediate. By including random errors and uncertainty boundaries, the confidence level (CL) for the classification can be provided. In case 2, the calibration changes the impedance grade from good to intermediate, while the uncertainty does not affect the classification for either fixture. In case 3, neither the calibration nor the uncertainty changes the impedance classification. In case 4, the calibration changes the impedance grade to bad, and including the uncertainty bounds, a quantitative CL can be established. In case 5, the calibration does not change the classification, but parts of the error ellipsoids are in grade bad, affecting the CL.

Experimental EIS demonstration for two fixtures

Based on the calibration of raw EIS data we evaluate the classification results of a single cylindrical cell at a selected frequency of 1500 Hz given the real part of the impedance and the uncertainty boundaries for two different fixtures. Table 2 shows the raw EIS data for the two fixtures, 12.23 mΩ and 12.43 mΩ, respectively. An arbitrarily selected impedance threshold of 12.3 mΩ is used for classification. Based on raw data, the cell would therefore be classified as good using fixture #1, and as bad using fixture #2. By correcting the systematic errors for both fixtures using the calibration procedure, the impedance values change to 12.33 mΩ and 12.48 mΩ, respectively. Considering the uncertainty boundaries and corresponding standard deviations, we get 12.33 mΩ ± 0.298 mΩ for fixture #1 (calibrated mean value and three standard deviations). Now a CL can be assigned to the classification, leading for fixture #1 only to 38.13% to be a good cell, and for fixture #2 only 58.07% to be a bad cell. Figure 4 shows the probability density function (pdf) with respect to the real part of the impedance at a single frequency point for the two fixtures. The good fixture (fixture #1) shows a narrow distribution around the calibrated mean value, while the bad fixture (fixture #2) has a broad impedance distribution. The selected threshold of 12.3 mΩ is indicated, as well as the CL for being classified as good and bad.

Table 2. Calibrated raw data and standard deviation derived from the uncertainty analysis. The CL for the classification is given for a single cylindrical cell at 1500 Hz and a selected threshold of 12.3 mΩ for two different fixtures.

Fixture	Raw value [mΩ]	Cal value [mΩ]	Standard deviation [mΩ]	Cal value ±3 standard deviations [mΩ]	Initial classification based on raw data	CL of classification based on cal value ±3*sigma
#1	12.23	12.33	0.0993	12.33 ± 0.298	Good	38.13% Good
#2	12.43	12.48	0.884	12.48 ± 2.652	Bad	58.07% Bad

Research Article
doi.org/10.1002/batt.202200524
Chemistry Europe
European Chemical Societies Publishing

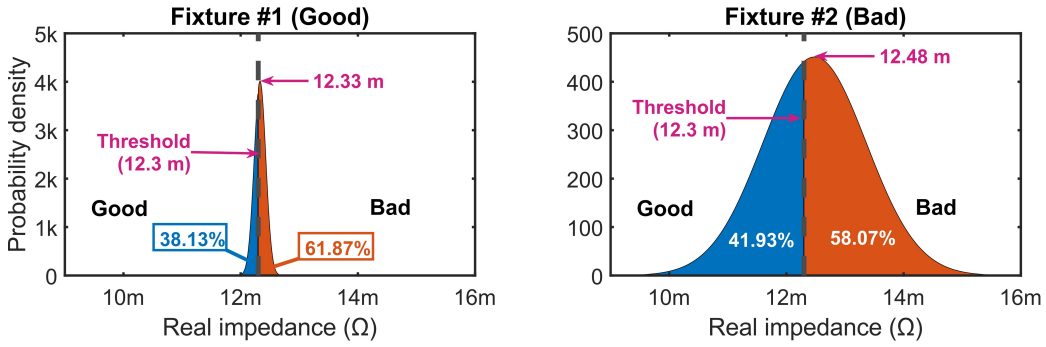

Figure 4. Uncertainty evaluation of the calibrated real part of the impedance of a single cylindrical cell at 1500 Hz using two different fixtures, a good fixture and a bad fixture. Left: the good fixture has a narrow error bound centered on the calibrated mean value of 12.33 mΩ, resulting in a CL of 38.13% to be a good cell. Right: the bad fixture shows a broader distribution with a calibrated mean value of 12.48 mΩ, resulting in a CL of 41.93% of it being a good cell.

EIS uncertainty over frequency

Calibration and uncertainty analysis is provided for the full frequency range of 150 mHz to 5 kHz. Figures 5A and 5B show the corresponding Nyquist plots for the two fixtures with the uncertainty given as error ellipsoids around each calibrated impedance measurement. The impedance measurements are performed at a total of 20 points in logarithmic intervals between 150 mHz and 5 kHz. The good fixture (#1) has smaller error bounds (see Figure 5A) compared to fixture #2 (see Figure 5B). Also, there is a slight variation in the error bounds with respect to the frequency, and the lowest error bounds are obtained at medium frequencies around 100 Hz. Figure 5A (inset figure) shows the error ellipsoids for the two fixtures superimposed at the selected frequency of 1500 Hz.

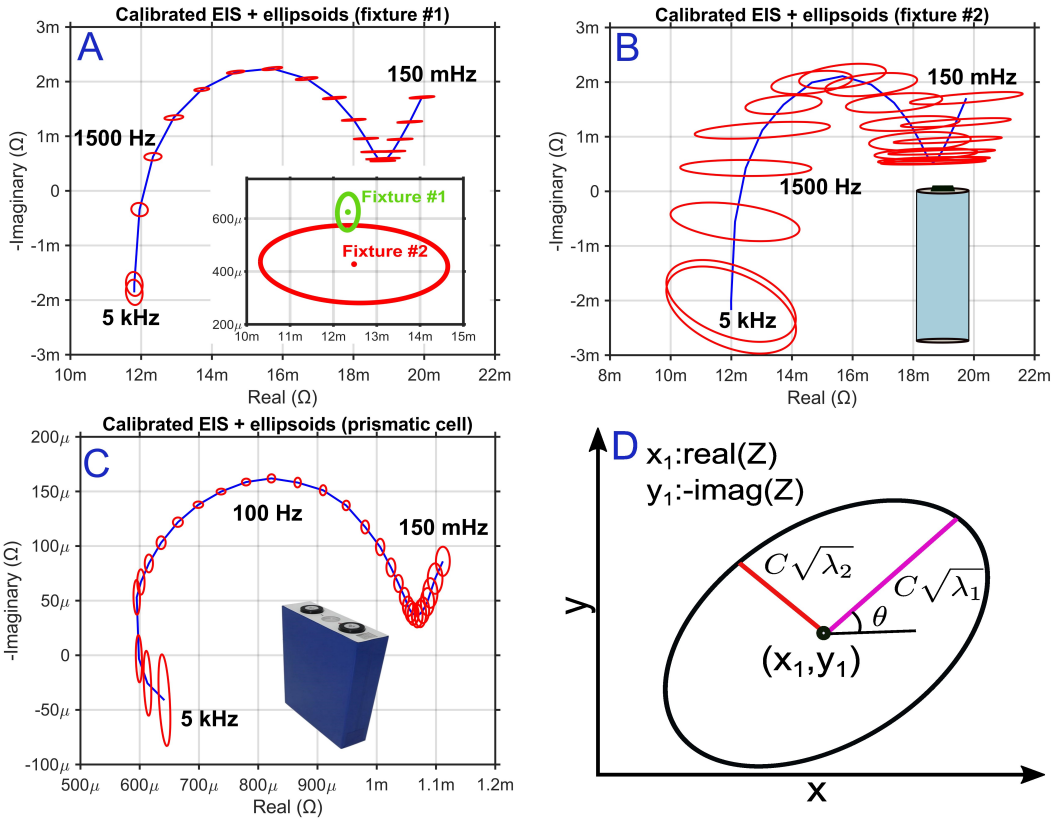

Figure 5. EIS uncertainty over the full frequency range of 150 mHz to 5 kHz at 95% CL. Calibrated impedance and error bounds using A) the good fixture #1 and B) the bad fixture #2. Inset in (A) shows the superposition of the error bounds of the two fixtures at 1500 Hz. C) The calibrated EIS result of a prismatic cell and the corresponding error ellipsoids. D) Error ellipsoid in the Nyquist plot. The ellipse is rotated by θ degrees, where θ is the angle between the horizontal axis and the covariance matrix's largest eigenvector. The length of the major and minor axes is proportional to the square root of the two eigenvalues of the uncertainty matrix.

Research Article
doi.org/10.1002/batt.202200524
Chemistry Europe
European Chemical Societies Publishing

The methods presented here are not limited to a specific measurement system or a specific battery type. The uncertainty and calibration methods work regardless of the battery cell chemistry, storage capacity, and form factors. Figure 5C shows the calibrated frequency-dependent impedance results and error boundaries for a prismatic cell with a nominal capacity of 24 Ah. The impedance values of the prismatic cells are lower compared to the cylindrical cell and are in the range of 600–1100 μΩ. Yet the proposed calibration and uncertainty characterization is performed effectively also on this low impedance level. The impedance uncertainty and calibration methods can also be applied to different battery cell chemistries, such as LFP (Lithium Iron-Phosphate) cathode chemistry. Figure 5D shows the calculation of the ellipsoids at each measurement point, where x and y are the coordinates of the real and the negative-imaginary components of the impedance. Equations (4) and (5) describe the shape of the ellipsoid where C is 2.4447 for the CL of 0.95 [$\chi_2^2(2.4447) = 0.95$] with χ_2^2 be the Chi-squared distribution with two degrees of freedom and $U = [u_1, u_2]$ is the largest eigenvector of the covariance matrix. Z is the measured impedance, and λ_1 and λ_2 are the covariance matrix's largest and smallest eigenvalues, respectively.[18] R is the rotation matrix which depends on the values of u_1 and u_2 according to Equation (5).

$$\begin{bmatrix} x(t) \\ y(t) \end{bmatrix} = R \begin{bmatrix} C\sqrt{\lambda_1}cos(t) \\ C\sqrt{\lambda_2}sin(t) \end{bmatrix} + \begin{bmatrix} real(Z) \\ -imag(Z) \end{bmatrix} \quad (4)$$

$$R = \begin{bmatrix} cos(\theta) & -sin(\theta) \\ sin(\theta) & cos(\theta) \end{bmatrix} \quad (5)$$
$$t = 0, \ldots, 2\pi \quad and \quad \theta = atan2(u_2, u_1)$$

Conclusion

This study shows how metrological EIS calibration and uncertainty analysis can improve cell classification. Experimental measurements are conducted on a commercial cylindrical cell using two different fixtures. The workflow includes a full calibration and uncertainty analysis in order to show the impact on the cell classification. Based on the uncertainty and corresponding error bounds, a confidence level was established for the classification. The uncertainty bounds are presented for the full EIS frequency spectrum ranging from 150 mHz to 5 kHz. For cell classification, the number of false positives and false negatives can be reduced using accurate confidence levels. EIS is typically done in the end-of-line test in cell production, and as such, the production efficiency can be improved with adequate calibration and uncertainty analysis. A quantitative life-cycle-analysis study will be done in future to determine savings on materials scrap and CO_2 reduction with the overall goal of making cell production greener. Additionally, while the classification in this study is based on a single frequency-point impedance measurement, future work will focus on including the whole EIS spectra and frequency-dependent error bounds in the analysis.

Acknowledgements

This work was supported in part by the European Union's Horizon 2020 Research and Innovation Program NMBP "NanoBat" under Grant 861962 and in part by the EMERALD project funded from the European Union's Horizon 2020 Research and Innovation Program under the Marie Sklodowska-Curie Grant Agreement under Grant 764479.

Conflict of Interest

The authors declare no conflict of interest.

Data Availability Statement

The data that support the findings of this study are available from the corresponding author upon reasonable request.

Keywords: calibration · cell classification · electrochemical impedance spectroscopy (EIS) · impedance calibration · lithium-ion battery · uncertainty

[1] Benchmark Mineral Intelligence, "Lithium ion battery pipeline breaks the 6 twh capacity barrier", can be found under https://source.benchmarkminerals.com/article/lithium-ion-battery-pipeline-breaks-the-6twh-barrier, **2022** (accessed 1 December 2022).
[2] L. Hoffmann, M. Kasper, M. Kahn, G. Gramse, G. Ventura Silva, C. Herrmann, M. Kurrat, F. Kienberger, *Batteries* **2021**, *7*, 64.
[3] M. Kasper, A. Leike, J. Thielmann, C. Winkler, N. Al-Zubaidi, R-Smith, F. Kienberger, *J. Power Sources* **2022**, *536*, 231407.
[4] X. Kong, G. L. Plett, M. Scott Trimboli, Z. Zhang, D. Qiao, T. Zhao, Y. Zheng, *J. Energy Storage* **2020**, *27*, 101085.
[5] a) A. L. Rue, P. J. Weddle, R. J. Kee, T. L. Vincent, in *2020 American Control Conference (ACC)*, **2020**, pp. 231–236; b) Z. Cui, L. Kang, L. Li, L. Wang, K. Wang, *Renewable Energy* **2022**, *198*, 1328–1340.
[6] a) R. Mingant, J. Bernard, V. Sauvant Moynot, A. Delaille, S. Mailley, J.-L. Hognon, F. Huet, *ECS Trans.* **2011**, *33*, 41; b) T. Osaka, D. Mukoyama, H. Nara, *J. Electrochem. Soc.* **2015**, *162*, A2529; c) Y. Guo, D. Yang, Y. Zhang, L. Wang, K. Wang, *Prot. Contr. Modern Power* **2022**, *7*, 40.
[7] a) H. P. G. J. Beelen, L. H. J. Raijmakers, M. C. F. Donkers, P. H. L. Notten, H. J. Bergveld, *Appl. Energy* **2016**, *175*, 128–140; b) X. Wang, X. Wei, Q. Chen, J. Zhu, H. Dai, *J. Energy Storage* **2019**, *26*, 100952.
[8] R. G. Jungst, G. Nagasubramanian, H. L. Case, B. Y. Liaw, A. Urbina, T. L. Paez, D. H. Doughty, *J. Power Sources* **2003**, *119–121*, 870–873, https://www.sciencedirect.com/science/article/abs/pii/S0378775303001939?via%3Dihub.
[9] a) H. Wang, L. He, J. Sun, S. Liu, F. Wu, in *Proceedings of 2011 6th International Forum on Strategic Technology*, Vol. 1, **2011**, pp. 261–264; b) J. Jiang, Z. Lin, Q. Ju, Z. Ma, C. Zheng, Z. Wang, *Energy Proc.* **2017**, *105*, 844–849.
[10] a) P. Iurilli, C. Brivio, V. Wood, *J. Power Sources* **2021**, *505*, 229860; b) P. Gasper, A. Schiek, K. Smith, Y. Shimonishi, S. Yoshida, *Cell Rep. Phys. Sci.* **2022**, *3*, 101184; c) Q. Zhang, D. Wang, E. Schaltz, D.-I. Stroe, A. Gismero, B. Yang, *J. Energy Storage* **2022**, *55*, 105386; d) Q. Zhang, C. G. Huang, H. Li, G. Feng, W. Peng, *IEEE Trans. Transp. Electrif.* **2022**, *8*, 4633–4645; e) M. Messing, T. Shoa, S. Habibi, *J. Energy Storage* **2021**, *43*, 103210.
[11] a) C. T. Love, M. B. V. Virji, R. E. Rocheleau, K. E. Swider-Lyons, *J. Power Sources* **2014**, *266*, 512–519; b) K. Takeno, M. Ichimura, K. Takano, J. Yamaki, S. Okada, *J. Power Sources* **2004**, *128*, 67–75.
[12] W. Waag, S. Käbitz, D. U. Sauer, *Appl. Energy* **2013**, *102*, 885–897.
[13] D. Li, D. Yang, L. Li, L. Wang, K. Wang, *Energies* **2022**, *15*, 6665.
[14] a) Y. Zhang, Q. Tang, Y. Zhang, J. Wang, U. Stimming, A. A. Lee, *Nat. Commun.* **2020**, *11*, 1706; b) J. Kim, L. Krüger, J. Kowal, *J. Energy Storage*

2020, *32*, 101841; c) X. Zhou, Z. Pan, X. Han, L. Lu, M. Ouyang, *J. Power Sources* **2019**, *417*, 188–192.
[15] a) T. F. Landinger, G. Schwarzberger, A. Jossen, in *2019 IEEE International Symposium on Electromagnetic Compatibility, Signal & Power Integrity (EMC + SIPI)*, **2019**, pp. 106–110; b) N. A. Z. R. Smith, M. Ragulskis, M. Kasper, S. Wagner, J. Pumsleitner, B. Zollo, A. Groebmeyer, F. Kienberger, *IEEE Trans. Instrum. Meas.* **2021**, *70*, 1–9; c) S. Mašláň, M. Šíra, T. Skalická, T. Bergsten, *IEEE Trans. Instrum. Meas.* **2019**, *68*, 1860–1869; d) M. Ortolano, L. Palafox, J. Kučera, L. Callegaro, V. D'Elia, M. Marzano, F. Overney, G. Gülmez, *Metrologia* **2018**, *55*, 499.
[16] A. Moradpour, M. Kasper, J. Hoffmann, F. Kienberger, *IEEE Trans. Instrum. Meas.* **2022**, *71*, 1–9.
[17] a) S. Davidsson Kurland, *Environ. Res. Commun.* **2020**, *2*, 012001; b) European Environment Agency, "Greenhouse gas emission intensity of electricity generation in Europe" can be found under https://www.eea.europa.eu/ims/greenhouse-gas-emission-intensity-of-1, **2022** (accessed 1 December 2022).
[18] C. D. Ghilani, *Adjustment Computations: Spatial Data Analysis*, Wiley, **2017**.

Manuscript received: December 2, 2022
Revised manuscript received: February 16, 2023
Version of record online: February 28, 2023